

# Journal of Materials Chemistry C

Accepted Manuscript



This is an *Accepted Manuscript*, which has been through the Royal Society of Chemistry peer review process and has been accepted for publication.

*Accepted Manuscripts* are published online shortly after acceptance, before technical editing, formatting and proof reading. Using this free service, authors can make their results available to the community, in citable form, before we publish the edited article. We will replace this *Accepted Manuscript* with the edited and formatted *Advance Article* as soon as it is available.

You can find more information about *Accepted Manuscripts* in the [Information for Authors](#).

Please note that technical editing may introduce minor changes to the text and/or graphics, which may alter content. The journal's standard [Terms & Conditions](#) and the [Ethical guidelines](#) still apply. In no event shall the Royal Society of Chemistry be held responsible for any errors or omissions in this *Accepted Manuscript* or any consequences arising from the use of any information it contains.

# Surface-initiated atom transfer radical polymerization of glycidyl methacrylate and styrene from boron nitride nanotubes

Cite this: DOI: 10.1039/x0xx00000x

Received 00th January 2012,  
Accepted 00th January 2012

DOI: 10.1039/x0xx00000x

www.rsc.org/

Muhammad Ejaz<sup>a†</sup>, Satish C. Rai<sup>b†</sup>, Kai Wang<sup>b</sup>, Karen Zhang<sup>b</sup>, Weilie Zhou<sup>b</sup> and Scott M. Grayson<sup>a\*</sup>

Boron nitride nanotubes (BNNTs) grafted with polyglycidyl methacrylate (PGMA) and polystyrene (PSt) brushes are described. This surface modification of BNNTs with polymer brushes is efficiently achieved involving only two steps: the introduction of benzyl bromide ATRP initiating sites on BNNTs by a one-step radical addition method and the surface initiated atom transfer radical polymerization (SI-ATRP) of GMA or St from the initiator immobilized BNNTs surface. The structure and properties of the resultant hybrid materials are characterized by Fourier transform infrared spectroscopy (FTIR), thermogravimetric analysis, scanning electron microscopy (SEM) and transmission electron microscopy (TEM). The FTIR analysis of hybrid materials shows infrared signals characteristic of the grafted polymers (PGMA and PSt) while SEM and TEM images clearly show the formation of polymer grafts on the BNNT surface.

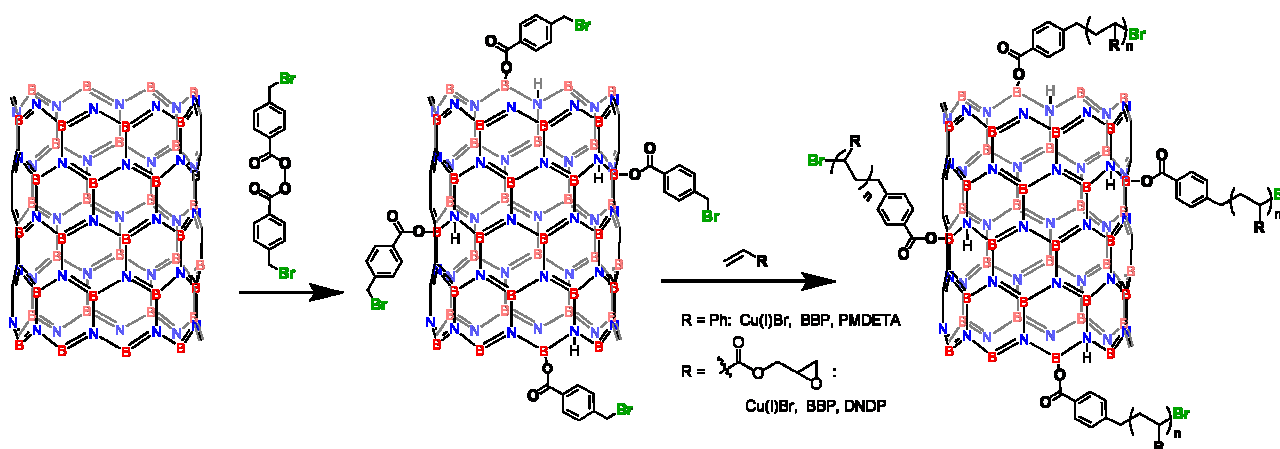
## Introduction

Boron nitride nanotubes (BNNTs) are the III–V homologues of carbon nanotubes (CNTs). Like CNTs, BNNTs exhibit exceptional durability, strength, and electronic properties, but they also exhibit a number of unique features including electrical insulating properties and increased thermal and chemical stability. Like CNTs, BNNTs exhibit a cylindrical structure that resembles “rolled-up” hexagonal graphitic sheets, except BNNTs consist of alternating N and B atoms rather than C atoms.<sup>1</sup> The length of a boron nitride nanotube can be greater than one micrometre while the typical diameter is on the order of nanometres. BNNTs have emerged as a promising new nanomaterial<sup>2</sup> with a range of remarkable properties, including excellent thermal conductivity,<sup>3</sup> high elastic modulus,<sup>4</sup> the high resistance to oxidation,<sup>5</sup> high structural stability,<sup>6</sup> useful electric properties,<sup>7</sup> and unique optical behavior<sup>8</sup> that complement those reported for CNTs. BNNTs also possess many of the superior properties of CNTs such as high material stiffness<sup>9</sup> and high heat conduction due to the effective phonon heat transfer.<sup>10</sup> These potentially useful physical properties make BNNTs an attractive alternative to CNTs for many applications that require chemical stability, high-temperature resistance, or electrical insulation. To date, BNNTs have seen application as composite materials,<sup>11</sup> luminescent nanomaterials,<sup>12</sup> and thermal conductive polymers.<sup>13</sup>

Recently, boron nitride (BN) based nanofillers such as BN nanoplatelets, BN nanosheets (BNNs) and BNNTs have attracted increased attention as a component in polymer composites for thermal dissipation<sup>14</sup> and epoxy resins were selected as the composite matrix because of their widespread use in the aerospace, automotive and electronic industries.<sup>15</sup> However, like CNTs,

unmodified BNNTs are not soluble in common solvents or compatible with bulk polymers, and therefore have a tendency to aggregate. Their poor interfacial interaction with polymer matrices inhibits their processability and reduces the quality of their nanocomposites.<sup>16</sup> Surface modification of the BNNTs is important to expand their applications in composite materials as well as biomedicine.<sup>17</sup> In addition to improving nanotube dispersibility during composite processing and fabrication, nanotube surface functionalization can vastly improve the interfacial interactions between the nanotube and bulk polymer if reactive functionalities such as epoxide rings, are present on the polymer grafts in order to covalently cross-link into the polymer network.<sup>18,19</sup> An external tensile load will be most efficiently transferred from the polymer onto the nanotubes only if a strong chemical bond exists between the two components of the composite.<sup>20</sup> The multiplicity of functionality that is exhibited by dense polymer grafts offers an increased degree of cross-linking into the polymer matrix that is ideal for a composite material.<sup>21</sup>

There are numerous functionalization schemes that have been reported for CNTs<sup>22,23</sup> but few have been reported so far for BNNTs.<sup>24</sup> This is primarily due to the inherent low chemical reactivity of the surface of well-crystallized BNNTs, and poor wetting properties which inhibit many traditional solution-based reactions.<sup>25</sup> The typically poor yields of BNNTs by conventional synthetic methods have also limited their availability for research on surface modification, though efforts to improve these yields are ongoing.<sup>14,26,27,28,29</sup> Recently, the surface modification of BNNTs has been explored to increase their dispersibility<sup>30</sup> including non-covalent surface adhesion techniques<sup>11,16,31,32</sup> and covalent sidewall



Scheme 1. Stepwise SI-ATRP process for grafting polymer brushes from BNNTs.

grafting.<sup>33,34,35</sup> Noncovalent strategies were achieved by adsorbing surfactants or polymers onto the BNNT surface, however, such adsorbed materials can desorb, resulting in nanotube aggregation. This problem is best overcome by covalent functionalization of BNNTs. While aggressive oxidation/sonication yields shortened nanotubes with increased solubility in water and other solvents,<sup>36</sup> more controlled oxidation provides largely intact nanotubes with surface functionalities<sup>37</sup>, which enable further surface modification.<sup>38</sup> Regardless, the most attractive method for tailoring the dispersibility of BNNTs is their covalent functionalization with polymer grafts as the diversity of polymers amenable to grafting offers a broad range of compatibility.

The surface modification of BNNTs by covalent attachment of polymer chains can be achieved via either a “grafting to” or “grafting from” approach. The “grafting to” approach, generally results in low graft densities due to steric complications. In the case of the “grafting from” approach, also known as surface initiated polymerization, the polymer is grown from initiator attached to the substrate and can yield much more densely packed polymer brushes. Among the different surface-initiated controlled polymerization techniques, surface-initiated atom transfer radical polymerization (SI-ATRP) has been most extensively used to produce dense polymer brushes on a range of different substrates.<sup>39</sup> In order to initiate ATRP from the relatively inert BNNT surface, graftable functionalities must be present. For example, Zhi et al.<sup>34</sup> introduced chloride groups onto BNNTs via amidation with chloroacetyl chloride of the adventitious free amino groups generated as structural impurities during their chemical vapour deposition synthesis. Because of the scarcity of these defects, the dry thickness of the polystyrene shell was relatively low, ranging from 0.8 to 5 nm due to defect concentration variations along the BNNTs. Recently Ejaz et al. developed a single step method for covalent immobilization of benzyl bromide ATRP initiators onto fully pyrolyzed carbon hard nanospheres (CHSs) by a radical fixation method. This approach provides a high density of attachment points resulting from the well-known fact that graphitic materials like carbon black are strong radical scavengers.<sup>40</sup> Like CHSs the BNNTs have many open-ended graphitic like flakes and therefore an analogous initiator fixation approach seemed promising.

In this work, we present a rapid covalent functionalization approach for the synthesis of well-defined high-density polymer brushes from the surface of BNNTs by SI-ATRP. This involves a two-step SI-ATRP procedure. The first step involves the thermolysis of a peroxide ATRP initiator precursor to generate in-situ benzyl

bromide capped ester radicals which functionalize the B atoms in BNNTs via oxygen radical attack<sup>41</sup>. The second step involves the graft polymerization of ATRP polymers from these surface-affixed initiators. Two monomers were explored: styrene (St) and glycidyl methacrylate (GMA), the latter of which exhibits epoxide functionalities to enable further reactivity. These resulting polymer grafts were thicker than those previously reported, and exhibited dispersibility in a wide range of organic solvents.

## Experimental

**Reagents** Styrene (St, 99%, Aldrich) and glycidyl methacrylate (GMA, 97+%, Fluka) were purified by passing through neutral alumina. Copper (I) bromide (CuBr, 99.99%, Aldrich) was purified as described in literature.<sup>32</sup> N,N,N',N'',N'''-pentamethyldiethylenetriamine (PMDETA, 99%, Aldrich), 4,4'-dinonyl-2,2'-bipyridine (DNNDP, 97%, Aldrich), 4-methylbenzyl bromide (MBB, 97%, Aldrich), sodium peroxide (97%, Sigma-Aldrich), 4-bromomethylbenzoyl bromide (BMBB, 96%, Sigma-Aldrich), and all other reagents were used as obtained from commercial sources. Boron powder (99%, Alfa Aesar), iron(II) oxide (FeO, 99.5%, Alfa Aesar) and magnesium oxide (MgO 99.95% Alfa Aesar) were used as received. The ATRP initiator precursor *bis*(4-bromomethylbenzoyl) peroxide (BBMBPO) was synthesized as described in literature.<sup>42,43</sup>

**Synthesis of BNNTs** The BNNTs were synthesized using boron oxide chemical vapour deposition (BOCVD) approach.<sup>29,30</sup> using a mixture of B, MgO and FeO in the molar ratio of 2:1:1. Briefly, a cleaned Si (100) substrate was coated with a 30 nm MgO layer by e-beam evaporation and used as the substrate for BNNTs synthesis. The precursor mixture in the above-mentioned ratio was placed at the centre of a horizontal tube furnace. The furnace temperature was raised to 1200 °C under 200–250 standard cubic centimetres per minute NH<sub>3</sub> flow at a tube pressure of 20 Torr and the reaction was carried out for 1 hour at which point the furnace was allowed to cool to room temperature. The “as-synthesized” BNNTs were then gently removed with a razor blade from the substrate to minimize contamination from the silicon substrate. The yield of BNNTs relative to the amount of boron precursor is roughly 1%.

**Immobilization of ATRP initiator onto BNNTs** 5.5 mg of powdered BNNTs were dispersed in 10 mL of toluene and sonicated for 20 min. 0.2 g (0.47 mmol) of BBMBPO was then added to the above mixture. After purging with Ar for an additional 30 minutes, the reaction was initiated by heating to 105 °C and stirred vigorously

under argon for 6 h. After wards, the modified BNNTs were collected by a repeated cyclic of dispersions by sonication into solvent, and recollections of the nanotubes by centrifugation. The solvent series used was first toluene, then dichloromethane, then tetrahydrofuran (THF), then methanol (MeOH) and finally anisole. The cleaned initiator-functionalized BNNTs in anisole were used directly for the graft polymerizations.

**ATRP of GMA** 5.50 mg of initiator-functionalized BNNTs were dispersed in a mixture of 6.00 g of GMA (42.2 mmol) and 12 g anisole in a 25 ml Schlenk flask equipped with a stir bar. After a 30 minute Ar purge, CuBr (6.05 mg, 0.042 mmol) was added to the above suspension under an Ar flow followed by addition of DNDP (34.34 mg, 0.084 mmol) and MBB (7.77 mg, 0.042 mmol), as free initiator. The flask was placed in a thermostatic oil bath at 70°C and the suspension was stirred for 24 h under Ar. The product was then diluted with THF. The PGMA-grafted BNNTs were isolated from free polymer by repeated dispersal in THF by bath sonication, centrifugation, and decanting the free polystyrene solution. Trace amounts of CuBr were removed by additional washes of MeOH/THF, aqueous NH<sub>4</sub>Cl/THF and H<sub>2</sub>O/THF. Finally the PGMA-grafted BNNTs were vacuum dried overnight. In a controlled experiment pristine BNNTs (without the initiator-modified surface) were subjected to identical GMA polymerization conditions as described above.

**ATRP of St** 5.50 mg of initiator-functionalized BNNTs were dispersed in a mixture of 6.00 g of St (57.0 mmol) and 6 g of anisole in a 25 ml Schlenk flask equipped with a stir bar. After a 30 minute Ar purge, CuBr (81.76 mg, 0.57 mmol) was added to the above suspension under an Ar flow followed by addition of PMDETA, (98.82 mg, 0.57 mmol) and MBB (10.55 mg, 0.057 mmol), as free initiator. The flask was placed in a thermostatic oil bath at 95 °C and the suspension was stirred for 25 h under Ar. The product was then diluted with THF and the PSt-grafted BNNTs were isolated from free polymer using the centrifugation/washing protocol described for the PGMA-grafted BNNTs. Finally the PSt-grafted BNNTs were vacuum dried overnight.

#### Instrumentation

<sup>1</sup>H NMR (400 MHz) spectra were obtained on a Varian Mercury spectrometer (Palo Alto, CA) using the TMS signal for calibration (0.00 ppm). Size exclusion chromatography was carried out on a Waters model 1500 series pump (Milford, MA) with a three-column series from Polymer Laboratories, Inc. consisting of PLgel 5 μm Mixed D (300 × 7.5 mm<sup>2</sup>), PLgel 5 μm 500 Å (300 × 7.5 mm<sup>2</sup>) and PLgel 5 μm 50 Å (300 × 7.5 mm<sup>2</sup>) columns. The system was fitted with a Model 2487 differential refractometer detector. THF was used as mobile phase (1 mL/min flow rate). The calculated molecular weight was based on retention time calibrated against linear polystyrene standards. Data was collected and processed using Precision Acquire software. Fourier transform infrared (FTIR) spectroscopy was performed using a NEXUS 670 FTIR SEP. The analyte was mixed with KBr and ground into a fine powder by mortar and pestle. The resulting solid mixture was pressed into a pellet for analysis. Thermogravimetric analysis (TGA) data was acquired using TA Instruments TGA 2950 Thermogravimetric Analyzer with heating rate of 10 °C per minute

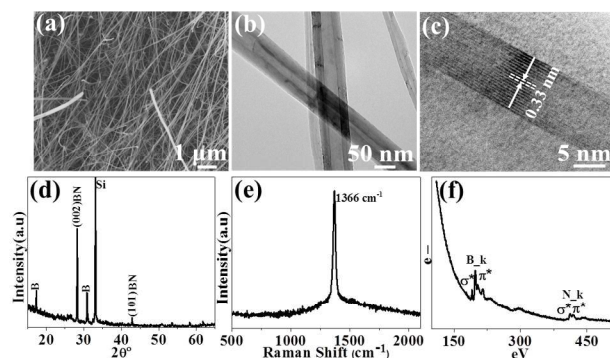


Fig.1. (a) Low magnification FESEM image of BNNTs synthesized by BOCVD (b) low and (c) high magnification TEM image (d) XRD spectrum of BNNTs on Si (100) substrate. (e) Raman spectrum of BNNTs at characteristic absorption and (f) EELS spectrum of BNNTs showing the distinct K-edge emission peaks of boron and nitrogen.

under N<sub>2</sub> atmosphere. Data was processed using TA Instruments Universal Analysis software. Transmission electron microscopy (TEM) data was collected with a JEOL 2010 operated at 200 kV. Field emission scanning electron microscopy (FESEM) data was obtained using LEO 1530VP, operated at 10 kV. Structural characterization data was obtained using PANalytical X-ray diffraction (XRD) (Xpert Pro-SAXS) and a Raman spectrometer from Princeton Instruments.

#### Results and discussion

In order to examine the viability of ATRP-grafted BNNTs, high purity BNNTs were first synthesized by the boron oxide chemical vapor deposition (BOCVD)<sup>27,44</sup> method. The mechanism behind the BOCVD approach involves the MgO and FeO catalyzed oxidation of boron to boron oxide at elevated temperatures. Interaction in the gas phase with ammonia results in the condensation of BNNTs onto the MgO coated-substrate.<sup>44</sup> However, the yield of this process is limited by the very small amount of solid boron which is optimal to yield the required vapor pressure for the growth of well-defined nanotubes. Generally, large amounts of boron will result in short BNNTs with large diameters.

The BNNTs were isolated from the substrate surface as a fluffy, white solid. FESEM imaging of these BNNT samples, as shown in Fig.1 (a), reveal that the BNNTs generally have a length of tens of micrometres and a diameter in the range of 50-100 nm. TEM analysis confirms the presence of tubular structures and the observed lattice fringes exhibit a lattice spacing of 0.33 nm which matches the inter-shell spacing (002) of hexagonal boron nitride (h-BN) (Fig.1(b-c)). The XRD spectrum, Fig.1(d), clearly exhibits the characteristic boron nitride (BN) signals while the sharp Raman absorbance at ~1366cm<sup>-1</sup> shown in Fig.1 (e) corresponds to the E<sub>2g</sub> band in-plane vibration mode of hexagonal BN. Electron energy loss spectroscopy (EELS) (Fig.1(f)) shows K edge emission peaks corresponding to B and N in the expected ~1:1 ratio.<sup>45</sup>

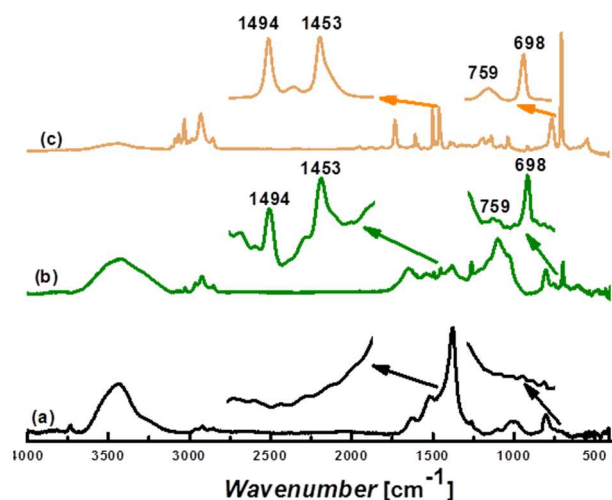


Figure 2. FTIR spectra of (a) pristine BNNTs, (b) BNNTs-PSt, and (c) PSt.

In this work a free radical addition reaction was employed to immobilize initiator onto the BNNT surface using an analogous technique to that reported for carbon hard spheres.<sup>40</sup> The peroxide bond within the BBMO reagent decomposes at 105 °C to generate free radicals. These free radicals are expected to react with localized  $\pi$  double bonds of the aromatic rings as well as any defective sites along the BNNTs surface. Similar radical attachment to BNNTs has been reported for other organic peroxides.<sup>41</sup> Using this radical fixation process, brominated benzyl groups were successfully attached onto the surfaces of BNNTs, providing multiple sides from which polymer grafts can be initiated by SI-ATRP.

The graft polymerizations of initiator functionalized BNNTs were carried out using both St and GMA monomers. While St was selected as a representative common ATRP monomer, GMA was specifically selected because of its utility in preparing BNNTs composites. The epoxide functionality of PGMA is highly reactive towards coupling with amines, alcohols, and other nucleophilic functional groups, providing an efficient means for crosslinking with a range of polymeric matrices for the generation of composite materials, including bisphenol-A epoxy resins, polycarbonates, etc. These PGMA-grafted BNNT composite materials could be of particular value for radiation-shielding materials, owing to the inherent neutron absorption properties of  $^{10}\text{B}$ .

The polymerization of both monomers was carried out in anisole, with the addition of free “sacrificial” initiator, 4-methylbenzyl bromide (MBB). The sacrificial initiators are typically used in SI-ATRP not only to provide a well-controlled graft polymerization but also to allow an indirect characterization of the grafted polymer chains. Although the molecular weight and the dispersity of the grafted polymer chains cannot be directly measured, because the free and the BNNT-bound initiating groups are of similar structure and exposed to the same conditions, it can be assumed that the polymers formed in solution will have a similar molecular weight profile to those grafted from the surface. This soluble polymer can be readily isolated and characterized by GPC, NMR, MALDI, etc.<sup>46</sup>

The GPC analysis for the PGMA grafting reaction yielded free polymer with number average molecular weight of 60 000 and a  $\text{Đ}$  of around 1.19 while the PSt polymerization yielded free polymer

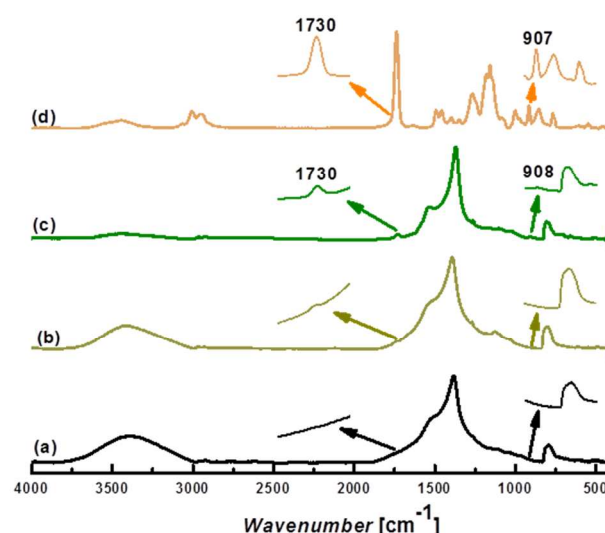


Figure 3. FTIR spectra of (a) pristine BNNTs (b) BNNTs, after control polymerization (c) BNNTs-PGMA and (d) PGMA.

with a number average molecular weight of 110 000 and a  $\text{Đ}$  of around 1.59. The relatively narrow dispersities confirm that both of the polymerizations were reasonably controlled and free polymer molecular weight suggests the grafted polymer chains had degrees of polymerization well beyond 100 repeating units.

Direct confirmation of the covalent polymer grafting to BNNTs could be obtained using FTIR. The FTIR spectrum of unfunctionalised BNNTs (Fig. 2a) is dominated by three characteristic peaks at around 809, 1369 and 1545  $\text{cm}^{-1}$ . The absorption band at  $\sim 1545 \text{ cm}^{-1}$  corresponds to the stretching of the hexagonal-BN network along the tangential directions of a BNNT. The intense  $\sim 1369 \text{ cm}^{-1}$  band is a result of the transverse optical mode of hexagonal-BN sheets that vibrates along the longitudinal or tube axis of a BNNT. Finally, the weak absorption at  $\sim 809 \text{ cm}^{-1}$  is associated with the out-of-plane radial buckling mode where boron and nitrogen atoms are moving radially inward or outward. After the graft polymerization of St onto BNNTs, the crude PS-grafted BNNTs samples were centrifuged, the solvent decanted, and the residue resuspended five times, to ensure that all of the unattached polymers had been removed. The purified PSt-BNNT samples exhibited all of the characteristic absorbances of PSt: 3030  $\text{cm}^{-1}$ , the C-H aromatic stretching; 2920  $\text{cm}^{-1}$ , the aliphatic C-H stretching;  $\sim 1453 \text{ cm}^{-1}$  and 1493  $\text{cm}^{-1}$ , the aromatic C=C ring stretches; and 600-800  $\text{cm}^{-1}$ , the phenyl ring stretching (Fig. 2b). These FTIR results confirm the successful grafting of PSt onto the BNNTs.

Analogous characterization could be used to confirm the grafting of PGMA onto the BNNTs. After isolating the PGMA grafted BNNTs, the characteristic, though weak, FTIR signals at 1732  $\text{cm}^{-1}$  for the carbonyl groups and 908  $\text{cm}^{-1}$  for the epoxy rings were observed (Fig. 3c). Caution must be used in relying too heavily on this FTIR data to prove surface grafting, given the weak signal of the polymer relative to the BNT substrate.<sup>47</sup> However, the presence of all of the characteristic signals expected for both the polystyrene and poly(glycidyl methacrylate) grafts provides complimentary evidence in addition to the TGA data, microscopy images and the observed improvement in solvent compatibility after grafting that are detailed below.

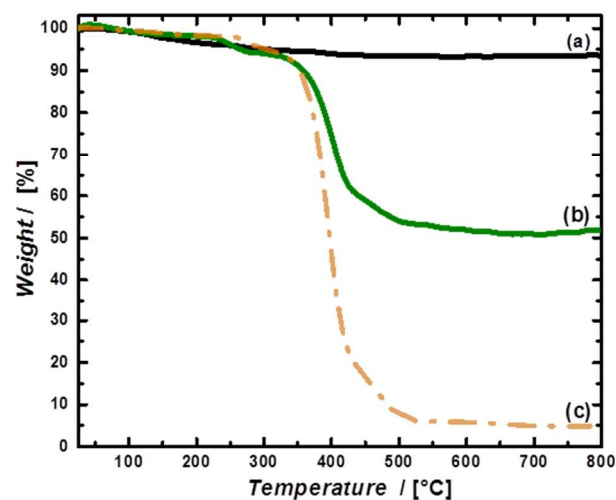


Figure 4. TGA curves of (a) pristine BNNTs (b) BNNTs-PGMA and (c) PGMA.

In order to provide further confirmation that the GMA grafts were covalently connected onto BNNTs and not merely physically adhering to the surface, a PGMA polymerization was carried out from the free initiator, in the presence of unmodified BNNTs. After the BNNTs were isolated using the analogous centrifugation/decanting/resuspension purification technique, their IR spectra failed to show any of the characteristic signals at  $1732\text{ cm}^{-1}$  or  $906\text{ cm}^{-1}$  (Fig.3b), suggesting that observed PGMA signals in the first sample was covalently attached rather than physically adsorbed onto the nanotubes. As additional evidence for substantial surface grafting, the dispersibility of both polymer grafted BNNTs in organic solvents, such as anisole, dichloromethane, tetrahydrofuran, toluene and dimethylformamide, were greatly enhanced for both PGMA and PSt grafts.

Thermogravimetric analysis was also used to provide quantitative data about the mass of grafted polymer relative to that of the BNNTs substrate. The pristine NNTs were fairly stable up to  $800\text{ }^{\circ}\text{C}$  without any significant loss of mass (Fig. 4a). A small but measurable weight loss of  $\sim 2.5\%$  starts at a temperature as low as  $150^{\circ}\text{C}$  and stabilizes to  $7\%$  around  $400^{\circ}\text{C}$ . This weight loss is believed to result from the hygroscopic nature of the MgO catalyst which may be present as a trace impurity from the removal of the BNNTs from the MgO coated substrate. The observe weight loss could be explained by the formation of  $\text{Mg}(\text{OH})_2$  in presence of environmental moisture (which completely dissociates to MgO and  $\text{H}_2\text{O}$  at  $332^{\circ}\text{C}$ ) as well as the low thermal stability ( $\sim 427^{\circ}\text{C}$ ) of MgO itself. Because of the robust thermal properties of BNNTs, they can survive temperatures as high as  $800\text{ }^{\circ}\text{C}$ . The PGMA grafted BNNTs, on the other hand, exhibited substantial mass losses around  $400\text{ }^{\circ}\text{C}$  ( $335\text{ }^{\circ}\text{C}$  onset point,  $405\text{ }^{\circ}\text{C}$  inflection point) (Fig. 4b), which corresponds closely with the temperature of decomposition that was observed for free PGMA (Fig 4c.). The relative mass of the polymer can be computed based upon the mass loss below  $800\text{ }^{\circ}\text{C}$ , relative to the total mass. This calculation yields a  $36\%$  mass loss, confirming a significant quantity of grafted PGMA via this radical fixation/SI-ATRP approach. Based on the TGA analyses, surface area of BNNTs and the presumed molecular weight of grafted polymer, (from the GPC data of the soluble polymer byproduct) the polymer graft density on the BNNTs was computed to be  $0.03\text{ chains/nm}^2$ .

Morphological characterization of PGMA grafted BNNTs was investigated using FESEM to directly observe the nanoscale

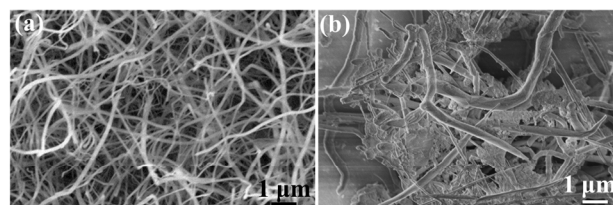


Figure 5. (a) and (b) low magnification FESEM image of pristine and PGMA-BNNTs respectively, showing an increase in the diameter of the BNNTs.

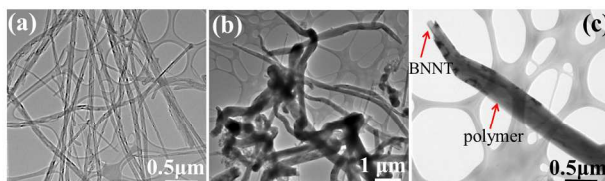


Figure 6. (a) Low magnification TEM image of pristine BNNTs; (b) low and (c) high magnification TEM images of PGMA grafted BNNTs, exposed tip and polymer layer is shown by arrow.

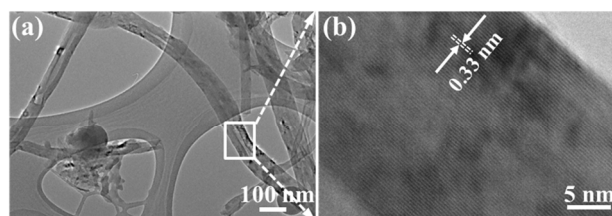


Figure 7. (a) Low magnification and (b) high magnification TEM image of BNNTs control polymerization revealing absence of any polymer wrapped around BNNTs surface.

morphology of PGMA grafted BNNTs. As can be clearly seen in the FESEM images (Fig. 5b), the BNNTs surfaces are completely coated by polymer and the diameter of BNNTs has significantly increased as compared to pristine BNNTs (Fig. 5a). Further characterization of the morphology and surface structure of PGMA-grafted BNNTs was carried out using TEM. A typical TEM image of polymer-grafted BNNTs is shown in Fig. 6b. It can be clearly seen that PGMA layer is wrapped around the BNNTs leading to an obvious increase in the overall diameter of BNNTs compared to the pristine BNNTs (Fig. 6a). By more closely examining the image of the grafted BNNTs (Fig. 6c), and comparing with the image of pristine BNNTs surface, the image of the grafted nanotubes shows a darker grey layer of PGMA layer around the sharply defined BNNT core. The BNNTs,

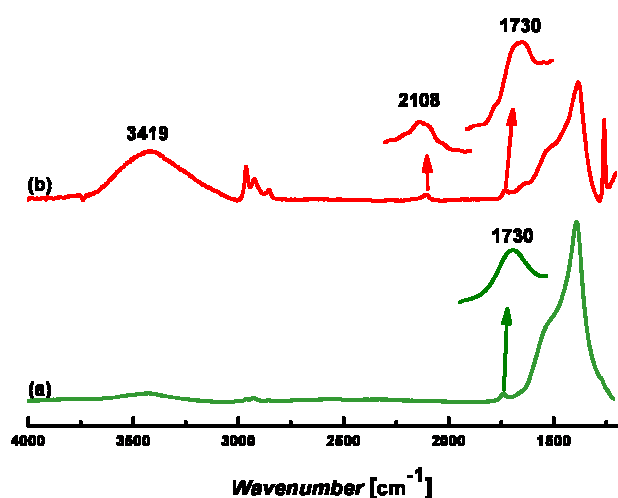


Figure 8. FTIR spectra of (a) BNNTs-PGMA (b) BNNTs-PGMA-OH/N<sub>3</sub>.

except the tips, are completely enveloped by a visible continuous and uniform smooth film of grafted PGMA as compared to pristine BNNTs (Fig. 6a). From these images the average thickness of the PGMA grafted films can be calculated. The average diameter of pristine BNNTs is ~70 nm, while the total diameter of PGMA-BNNTs varies from tip to base of grafted BNNTs with values of ~130 nm at the tip and ~250 nm at the base. This corresponds to a total polymer graft thickness of between ~30 nm at tip and ~90 nm along the body of the nanotube. To further rule out the possibility of physical adsorption of PGMA on the BNNTs surface, TEM was used to examine the pristine BNNTs used in the control polymerization experiment (Fig. 7). It was found that the pristine BNNTs, obtained after the control GMA polymerization experiment, do not show any signs of PGMA on their surface (Fig. 7a) similar to fresh BNNTs (Fig. 6a). In addition, the high resolution TEM of BNNTs from this control polymerization experiment (Fig. 7b) is similar to those of fresh BNNTs (Fig. 1c). FTIR data for the control BNNTs also exhibit no sign of polymer. The results of these detailed microscopy studies verify not only the presence of a thick layer of polymer after the radical fixation/SI-ATRP protocol, but the control studies also confirm that this polymer layer is attached covalently.

In order to confirm the presence of epoxide rings on the grafted BNNTs, the PGMA modified BNNTs were treated with sodium azide according to literature procedures to generate the azido alcohol repeating unit.<sup>48,49</sup> The FTIR spectra after reaction of PGMA-BNNTs with NaN<sub>3</sub> (figure 8) exhibit the distinct signal of free azides in the product (2100 cm<sup>-1</sup>) as well as an increase in the hydroscopic nature of the grafted BNNTs (3200-3600 cm<sup>-1</sup>) due to the hydroxyl groups on the sidechains. This confirms not only the presence of polymer grafts on the BNNTs, but the ability to carry out subsequent reactions with the epoxy sidechains.

## Conclusions

Using a 1-step radical addition reaction the benzyl bromide ATRP initiators were successfully introduced onto the surfaces of BNNTs. In a second step, the initiator groups were used to carry out SI-ATRP of St and GMA on BNNT. FT-IR, TGA, TEM and SEM were used to verify the grafting of both PGMA and PST onto the surface of the BNNTs. These results validate the utility of this 2-step grafting approach for the efficient preparation of polymer-grafted

BNNTs and confirm the value of this synthetic tool for preparing BNNTs for incorporation into polymer-based nanocomposites.

## Acknowledgements

This work was supported by Tulane University and BP/Gulf of Mexico Research Initiative (2012-II-798). We thank Dr. Kai Sun from University of Michigan for HRTEM and EELS scan and Dr. Gabriel Caruntu from University of New Orleans for Raman measurement.

## Notes and references

<sup>a</sup>Tulane University, Chemistry Department, New Orleans, LA, USA

<sup>b</sup>University of New Orleans, Advanced Materials Research Institute, New Orleans, LA, USA

\*Corresponding author Tel.: 1-504-862-8135; -fax: +1-504-865-5596

E-mail address; sgrayson@tulane.edu

¶ These authors contributed equally to this work.

1. D. Golberg, Y. Bando, C. Tang, and C. Zhi, *Adv. Mater.*, 2007, **19**,
2. N. Chopra, R. Luyken, K. Cherrey, V. Crespi, M. Cohen, S. Louie, and A. Zettl, *Science*, 1995, **269**, 966–967.
3. Y. Xiao, X. H. Yan, J. X. Cao, J. W. Ding, Y. L. Mao, and J. Xiang, *Phys. Rev. B*, 2004, **69**, 205415.
4. N. G. Chopra and A. Zettl, *Solid State Commun.*, 1998, **105**, 297–300.
5. Y. Chen, J. Zou, S. J. Campbell, and G. Le Caer, *Appl. Phys. Lett.*, 2004, **84**, 2430–2432.
6. W. Mickelson, S. Aloni, W. Q. Han, J. Cumings, and A. Zettl, *Science*, 2003, **300**, 467–469.
7. A. Rubio, J. Corkill, and M. Cohen, *Phys. Rev. B*, 1994, **49**, 5081–5084.
8. J. S. Laurent, R. Arenal, F. Ducastelle, A. Loiseau, M. Cau, B. Attal-Tretout, E. Rosencher, and L. Goux-Capes, *Phys. Rev. Lett.*, 2005, **94**, 037405.
9. K. N. Kudin, G. E. Scuseria, and B. I. Yakobson, *Phys. Rev. B*, 2001, **64**, 235406.
10. C. W. Chang, A. M. Fennimore, A. Afanasiev, D. Okawa, T. Ikuno, H. Garcia, D. Li, A. Majumdar, and A. Zettl, *Phys. Rev. Lett.*, 2006, **97**, 085901.
11. C. Y. Zhi, Y. Bando, C. C. Tang, R. G. Xie, T. Sekiguchi and D. Golberg, *J. Am. Chem. Soc.*, 2005, **127**, 15996–15997.
12. L. W. Yin, Y. Bando, D. Golberg, A. Gloter, M. S. Li, X. L. Yuan, and T. Sekiguchi, *J. Am. Chem. Soc.*, 2005, **127**, 16354–16355.
13. T. Terao, Y. Bando, M. Mitome, C. Zhi, C. Tang, and D. Golberg, *J. Phys. Chem. C*, 2009, **113**, 13605–13609.
14. D. Golberg, Y. Bando, Y. Huang, T. Terao, M. Mitome, C. Tang, and C. Zhi, *ACS Nano*, 2010, **4**, 2979–2993.
15. J. K. H. Teo, C. L. Toh, and X. Lu, *Polymer*, 2011, **52**, 1975–1982.
16. S. Velayudham, C. H. Lee, M. Xie, D. Blair, N. Bauman, Y. K. Yap, S. A. Green, and H. Liu, *ACS Appl. Mater. Interfaces*, 2010, **2**, 104–110.
17. G. Ciofani, S. Danti, G. G. Genchi, B. Mazzolai, and V. Mattoli, *Small*, 2013, **9**, 1672–1685.
18. C. Velasco-Santos, A. L. Martinez-Hernandez, and V. M. Castano, *Compos. Interfaces*, 2005, **11**, 567–586.
19. A. Eitan, K. Y. Jiang, D. Dukes, R. Andrews, and L. S. Schadler, *Chem. Mater.*, 2003, **15**, 3198–3201.
20. G. L. Hwang, Y. T. Shieh, and K. C. Hwang, *Adv. Funct. Mater.*, 2004, **14**, 487–491.
21. P. Singh, S. Campidelli, S. Giordani, D. Bonifazi, A. Bianco, and M. Prato, *Chem. Soc. Rev.*, 2009, **38**, 2214–2230.
22. Y. P. Sun, K. F. Fu, Y. Lin, and W. J. Huang, *Accounts Chem. Res.*, 2002, **35**, 1096–1104.
23. D. Tasis, N. Tagmatarchis, A. Bianco, and M. Prato, *Chem. Rev.*, 2006, **106**, 1105–1136.
24. C. Y. Zhi, Y. Bando, C. C. Tang, S. Honda, K. Sato, H. Kuwahara, and D. Golberg, *Angew. Chem.-Int. Ed.*, 2005, **44**, 7929–7932.
25. L. H. Li and Y. Chen, *Langmuir*, 2010, **26**, 5135–5140.
26. Y. Huang, J. Lin, C. Tang, Y. Bando, C. Zhi, T. Zhai, B. Dierre, T. Sekiguchi, and D. Golberg, *Nanotechnology*, 2011, **22**, 145602.
27. C. H. Lee, J. Wang, V. K. Kayatsha, J. Y. Huang, and Y. K. Yap, *Nanotechnology*, 2008, **19**, 455605.

28. C. Tang, Y. Bando, T. Sato, and K. Kurashima, *Chem. Commun.*, 2002, 1290–1291.
29. C. Zhi, Y. Bando, C. Tang, H. Kuwahara, and D. Golberg, *Adv. Mater.*, 2009, **21**, 2889–2893.
30. C. Y. Zhi, Y. Bando, C. C. Tang, Q. Huang, and D. Golberg, *J. Mater. Chem.*, 2008, **18**, 3900–3908.
31. Z. Gao, C. Zhi, Y. Bando, D. Golberg, and T. Serizawa, *J. Am. Chem. Soc.*, 2010, **132**, 4976–4977.
32. S. Pal, S. R. C. Vivekchand, A. Govindaraj, and C. N. R. Rao, *J. Mater. Chem.*, 2007, **17**, 450–452.
33. S. Y. Xie, W. Wang, K. a. S. Fernando, X. Wang, Y. Lin, and Y. P. Sun, *Chem. Commun.*, 2005, 3670–3672.
34. C. Zhi, Y. Bando, C. Tang, H. Kuwahara, and D. Golberg, *J. Phys. Chem. C*, 2007, **111**, 1230–1233.
35. C. Y. Zhi, Y. Bando, C. C. Tang, S. Honda, K. Sato, H. Kuwahara, and D. Golberg, *Angew. Chem.-Int. Ed.*, 2005, **44**, 7932–7935.
36. C. Zhi, N. Hanagata, Y. Bando, and D. Golberg, *Chem. Asian J.*, 2011, **6**, 2530–2535.
37. X. J. Dai, Y. Chen, Z. Chen, P. R. Lamb, L. H. Li, J. du Plessis, D. G. McCulloch, and X. Wang, *Nanotechnology*, 2011, **22**, 245301.
38. G. Ciofani, G. G. Genchi, I. Liakos, A. Athanassiou, D. Dinucci, F. Chiellini, and V. Mattoli, *J. Colloid Interface Sci.*, 2012, **374**, 308–314.
39. M. Ejaz, S. Yamamoto, K. Ohno, Y. Tsujii, and T. Fukuda, *Macromolecules*, 1998, **31**, 5934–5936.
40. M. Ejaz, B. Sunkara, L. Kamboj, J. He, V. T. John, N. S. Pesika, and S. M. Grayson, *J. Polym. Sci. Part -Polym. Chem.*, 2013, **51**, 3314–3322.
41. T. Sainsbury, A. Satti, P. May, Z. Wang, I. McGovern, Y. K. Gun'ko, and J. Coleman, *J. Am. Chem. Soc.*, 2012, **134**, 18758–18771.
42. B. Hazer, *Eur. Polym. J.*, 1990, **26**, 1167–1170.
43. Y. Sun, Y. Wu, L. Chen, Z. Fu, and Y. Shi, *Polym. J.*, 2009, **41**, 954–960.
44. C. H. Lee, M. Xie, V. Kayastha, J. Wang, and Y. K. Yap, *Chem. Mater.*, 2010, **22**, 1782–1787.
45. C.-Y. Su, W.-Y. Chu, Z.-Y. Juang, K.-F. Chen, B.-M. Cheng, F.-R. Chen, K.-C. Leou, and C.-H. Tsai, *J. Phys. Chem. C*, 2009, **113**, 14732–14738.
46. M. Ejaz, Y. Tsujii, and T. Fukuda, *Polymer*, 2001, **42**, 6811–6815.
47. C. Zhi, Y. Bando, T. Terao, C. Tang, H. Kuwahara, and D. Golberg, *Chem. Asian J.*, 2009, **4**, 1536–1540.
48. X. Lian, D. Wu, S. Song, and H. Zhao, *Macromolecules*, 2010, **43**, 7434–7445.
49. B. Zhang, H. Zhang, R. Elupula, A. M. Alb and S. M. Grayson, *Macromol. Rapid Comm.*, 2014, **35**, 146–151.

An efficient two-step polymer grafting procedure is developed for the functionalisation of boron nitride nanotubes. Using surface initiated atom transfer radical polymerisation, dense grafts of poly(glycidyl methacrylate) and polystyrene were successfully grown from the nanotube surface.

